

Chapter 3

NMR Studies in Diammonium Hexafluorozirconate $(\text{NH}_4)_2\text{ZrF}_6$

3.1 Introduction

NMR is one of the most powerful local probes to investigate mobility and internal motions in solids and is therefore used to study molecular dynamics, (i.e., determination of associated correlation times (τ_c) and activation energies (E_a)), phase transitions (if any) and mobility of conducting species in variety of inorganic solids. The temperature dependence of the spin lattice relaxation time gives information on the dynamics of the molecular groups present. The theory developed by Bloembergen, Purcell and Pound, known as BPP theory [1] has been quite successful in explaining the observed spin lattice relaxation time measurements. Many of the ammonium based inorganic solids exhibit superionic conduction. The diffusion of ammonium ions in these superionic solids is known to be a major contribution to ionic conductivity. Our interest is to study ammonium ion dynamics in these compounds using NMR second moment and spin-lattice relaxation time (T_1) measurements. Different types of motion like the reorientation, torsional oscillations, the spin rotation [2], diffusion [2-4], tunnelling [5-9], etc., are observed at different temperature ranges. Deviations in the T_1 behaviour from the BPP theory indicate relaxation mechanisms other than molecular reorientational dynamics. For example, quantum rotational tunnelling process is invoked to explain T_1 results in $(\text{NH}_4)_2\text{PtBr}_6$ [10-12] and order-disorder effects in NH_4Cl [13]. tunnelling has been invoked to explain multiple T_1 minima [5,14,15] and additional sidebands [5] at low temperatures in many ammonium compounds.

Ammonium salts of the type A_2BX_6 , ($\text{A} = \text{NH}_4, \text{N}(\text{CH}_3)_4$ etc, $\text{B} = \text{Se Pt, Pb, Te, Sn, Ti}$ and $\text{X} = \text{Cl, Br, I}$) with antifluorite structure, consists of a large anion compared to the cation, which is not highly charged. It is found that the ammonium ion performs isotropic reorientation about the symmetry axes and contributes to the ^1H spin lattice relaxation through the intra molecular dipole-dipole interaction [16-17]. In these compounds, the motion of the NH_4 ion is hindered by a low potential barrier (0.6 - 4.0 kcal/mol) [18] and the activation energy increases with decreasing lattice dimension [19]. The cations, like $\text{NH}_4, \text{N}(\text{CH}_3)_4$ etc. in these compounds, occupy the spacious cages formed by MX_6^{2-} octahedra located at the corners and the face centers of the cubic structures resulting in low activation energies. Proton magnetic resonance in systems like

NH_4Br , NH_4I , NH_4SCN , $(\text{NH}_4)_2\text{CrO}_4$ and NH_4NO_3 at 1.8 K gives evidence of quantum mechanical tunnelling [5]. Proton spin lattice relaxation behaviour of ammonium ion in $(\text{NH}_4)_2\text{GeF}_6$ at 8 MHz below 15 K is explained by quantum tunnelling [14]. T_1 studies at low temperatures, in various deuterated compounds are also explained by tunnelling. Study of quantum tunneling in various compounds using inelastic neutron scattering has been reviewed by Prager [20], while that using NMR has been reviewed by Srinivasan [21], Clough [22 - 24] and Horsewill [25 - 26]. The study of the absorption spectra and relaxation times of proton have given useful information on the tunnel splitting of NH_4 ion at low temperatures [5, 27 - 28]. It has been shown that the tunneling of NH_4 affects the spin lattice relaxation time (T_1) in various striking ways [29 - 32]: (1) observation of non-exponential relaxation, (2) multiple T_1 minima at low temperatures. Mechanism of the spin lattice relaxation at low temperatures is complicated because of the coupling between the librational mode of NH_4 ion and the phonon system.

Tuohi et al [33] have observed anomalous T_1 behaviour in $(\text{NH}_4)_2\text{PbCl}_6$ which are attributed to quantum tunneling. Svare [7] has developed a theory to explain the temperature dependence of average tunnel frequency in $(\text{NH}_4)_2\text{PbCl}_6$ in the range 15 to 40 K. He has found that very short life- time (2 ps) in the first excited torsional state of NH_4 as reason for temperature dependence of tunnel frequency. Temperature dependence of the average tunnel splitting (ω_t) of the ammonium ion in $(\text{NH}_4)_2\text{PbCl}_6$ has been determined as a function of temperature by observing the tunneling minima in proton spin lattice relaxation time which is found to vary from 47.6 MHz (at 4.2 K) to 12.5 MHz (at 50.6 K) [34 - 35]. Non-exponential recovery has been observed in the T_1 measurements in NH_4NO_3 below 20 K and spin conversion was observed below 4 K [36]. Proton T_1 and $T_{1\rho}$ have been studied by Svare et al [37] in powders of $(\text{NH}_4)_2\text{MCl}_6$ where $M = \text{Pd}, \text{Pt}, \text{Te}, \text{Ru}, \text{Ti}, \text{Ir}$ and Re from 40 to 300 K. The activation energies E_a for NH_4 motion are found to lie in the range (0.6 – 4.5 kcal/mol) and E_a is a linear function of the lattice dimension for the cubic hexachlorides. These very extensive NMR investigations of the ammonium hexahalozirconates have suggested that it would be instructive to investigate Diammonium hexafluorozirconate (Ammonium zirconate), in which the reorientation of both cation and anion groups are present.

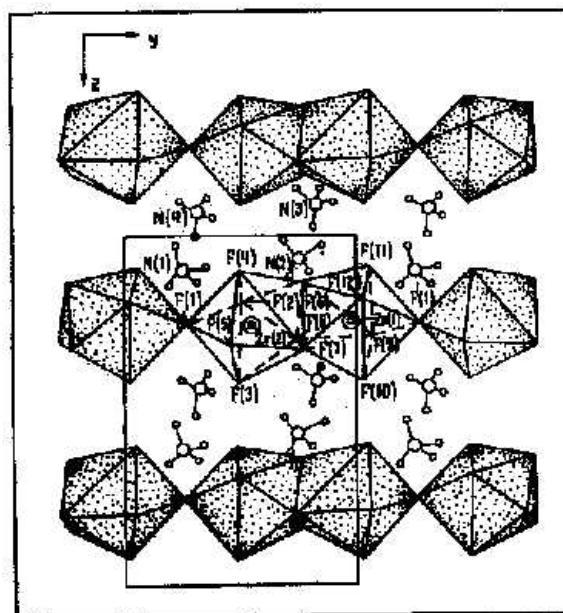
In the present study, proton and fluorine spin lattice relaxation time (T_1) measurements are undertaken in Ammonium zirconate for the following reasons: (1) the two possible reorienting groups like NH_4 and ZrF_6 are well suited for NMR studies. (2) The importance of proton-fluorine dipolar interactions can be understood. Spin lattice relaxation time measurements, as a function of temperature would provide more reliable activation energies for the processes governing the relaxation in explaining the superionic conductivity and translational diffusion properties. Further Ammonium zirconate is a promising candidate for technological applications viz., in organometal catalyst compositions, to increase the polymerization activity with silica-gel supported chromium oxide catalysts, as fluorinating agent, for curable resin composition, as an excellent corrosion resistant material and in making lithographic printing plates [38].

In the present study, commercially available ammonium zirconate from Aldrich Chemical Co., (39,729-6) is used directly without further purification. The compound is finely powdered and vacuum-sealed into glass ampoules of 5 mm diameter in helium atmosphere and then used for NMR measurements.

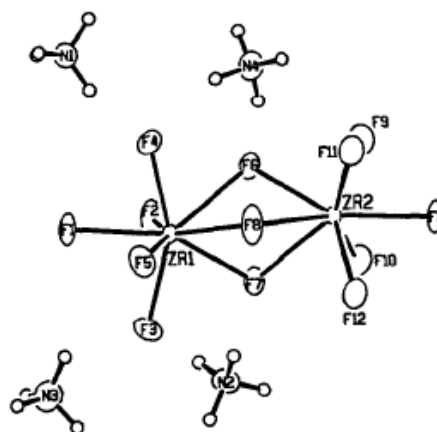
3.2 Earlier studies

Allan Zalkin et al have reported the room temperature crystal structure of Ammonium zirconate [39]. The crystal structure of Ammonium zirconate indicates that, it consists of Zr_2F_{12} units extended in infinite chains along the c-axis and ammonium ions are hydrogen bonded in a complex three dimensional network to these chains. Each Zr atoms are coordinated to eight F atoms. A triangle of three F atoms, at the center of the Zr_2F_{12} group, is sandwiched between two Zr atoms [39]. $(\text{NH}_4)_2\text{ZrF}_6$ has also been studied using wide line NMR, dc conductivity, IR, Raman and other techniques [28, 40-49]. The infrared and Raman active NH_4 -vibrations in ammonium zirconate [40] are found to occur at relatively high wave numbers, which is characterized by moderate to weak hydrogen bonds [50]. Kavun et al [47] have estimated the activation energy for the transition of ions to local (diffusion) motions using the formula $E_a = 155 - T_c$ kJ/mol. T_c in this equation is taken to be the temperature (in Kelvin) of the beginning of the NMR

spectrum narrowing or the appearance of a narrow component. Lalowicz et al [28] have carried out the proton NMR line shape calculation and analysis at 4.2 K for ammonium zirconate and attributed their results to the tunneling rotations of the ammonium ion. Figure 3.1 shows the projection of the crystal structure of the ammonium hexafluorozirconate and the ORTEP plot. The characteristic parameters of ammonium hexafluorozirconate are given in Table 3.1.



(a)



(b)

Figure 3.1 (a) Projection of the crystal structure of $(\text{NH}_4)_2\text{ZrF}_6$ on the yz -plane [41]. (b) ORTEP drawing showing the atomic numbering scheme. 50% probability ellipsoids are shown [39].

Table 3.1 Characteristic parameters of Ammonium zirconate [39]

Structure	Orthorhombic
Space group	Pca2 ₁
Cell dimension	a = 13.398 Å
	b = 7.739 Å
	c = 11.680 Å
Density	2.65 g cm ⁻³
Zr-F (1)	2.02 Å
Zr-F (2)	2.343 Å

3.3 Results and discussion

Spin lattice relaxation time

Figure 3.2 shows the variation of ¹H and ¹⁹F NMR spin lattice relaxation times (T₁) at 21.34 MHz with inverse temperature (1000/T) over the entire temperature range studied. The magnetization recovery profiles for both the nuclei (¹H and ¹⁹F) are found to be exponential within experimental errors throughout the temperature region studied.

3.3.1 Analysis of ¹H NMR T₁

At room temperature, T₁ value is about 38 ms and on increasing the temperature, T₁ starts decreasing up to 395 K, above which it reduces sharply to less than a millisecond. In the same temperature region, FID duration also increases several times as the temperature is increased from 388 K to 410 K. On decreasing the temperature from room temperature, initially T₁ increases and shows a maximum of about 48 ms around 240 K. Below 240 K, T₁ decreases and follows through a minimum of about 6.6 ms around 160 K and then increases to about 11 ms at 146 K. Below this temperature, T₁ decreases to about 8.8 ms and remains constant (within experimental error) till about 50 K. Below 50 K, T₁

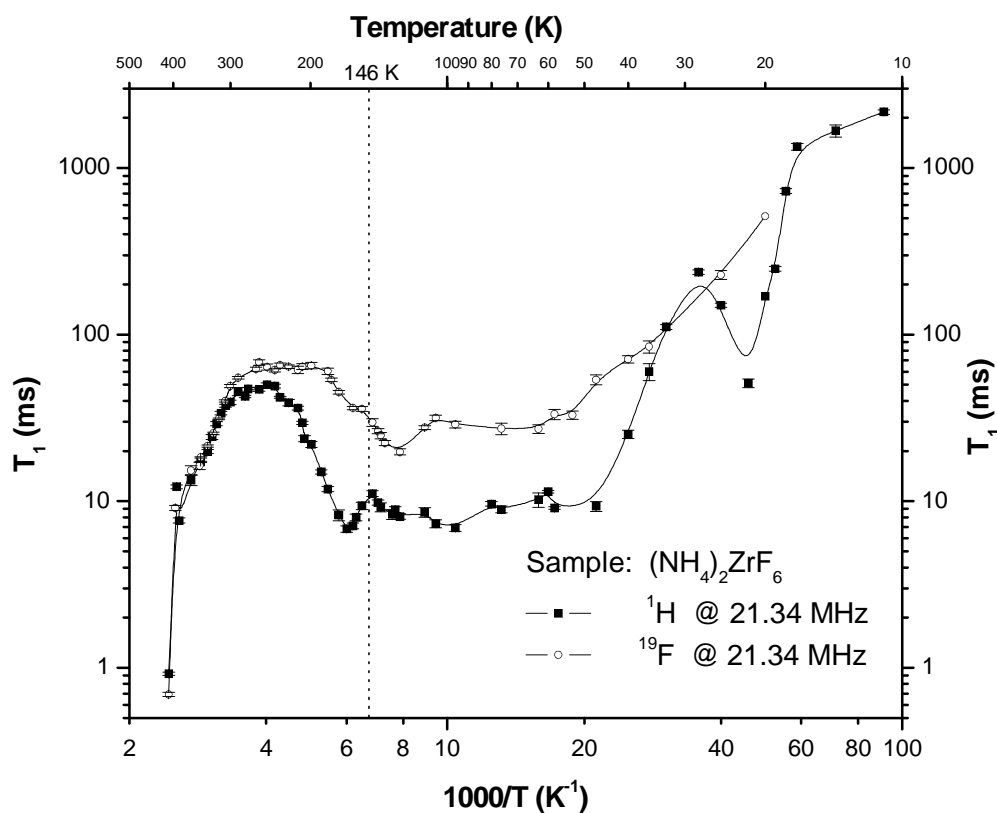


Figure 3.2 ^1H , ^{19}F NMR T_1 data at 21.34 MHz (with error bars) of Ammonium zirconate in the entire temperature range studied. The solid line is guide to the eye.

again increases and below 30 K, it shows another minimum of 51 ms around 22 K. Below 20 K, T_1 increases monotonically to a few seconds till the lowest temperature of measurement (11 K) in the present investigation. The T_1 data are analyzed in three parts: the High Temperature (HT) region (410 - 240 K), the Intermediate Temperature (IT) region (240 - 146 K) and the Low Temperature (LT) region (146 – 11 K).

3.3.1.1 High Temperature (HT) region (410 - 240 K)

Before the T_1 analysis, we present some details of second moment studies [41] of both proton and fluorine for better comparison as shown in Fig. 3.3 in the same compound Ammonium zirconate. In the temperature region 135-290, the ^1H NMR spectra of Ammonium zirconate showed a single and comparatively broad line [41]. Above 295 K,

a narrow component appears in the center of the spectrum and the second moment also decreases to 2.3 G^2 from 5.5 G^2 . Above 370 K , ^1H NMR line width starts decreasing and finally reaches to a negligible value (0.15 G) around 400 K .

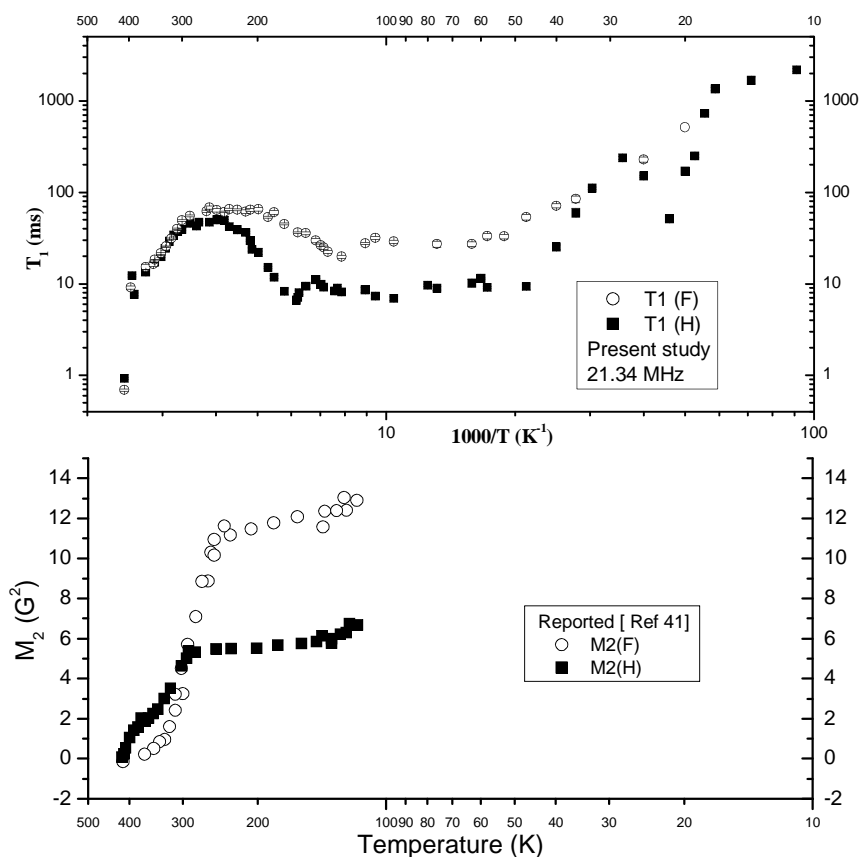


Fig 3.3 NMR Spin lattice relaxation times and second moments [41] of both proton (closed squares) and fluorine (open circles) for Ammonium zirconate in the entire temperature region of measurements.

Both decrease in T_1 and narrowing of the NMR signal shows the diffusion of both NH_4 and F ions through the lattice. High ionic conductivity above 400 K observed by Kavun et al [47] supports this. ^1H NMR line width above 400 K , measured by the same authors, reaches a limit of modulation width, as discussed above, indicating the diffusion of ammonium ions. The observed maximum in T_1 in the present study around room temperature may be attributed to the competition between diffusion and reorientational motion of the NH_4 ions.

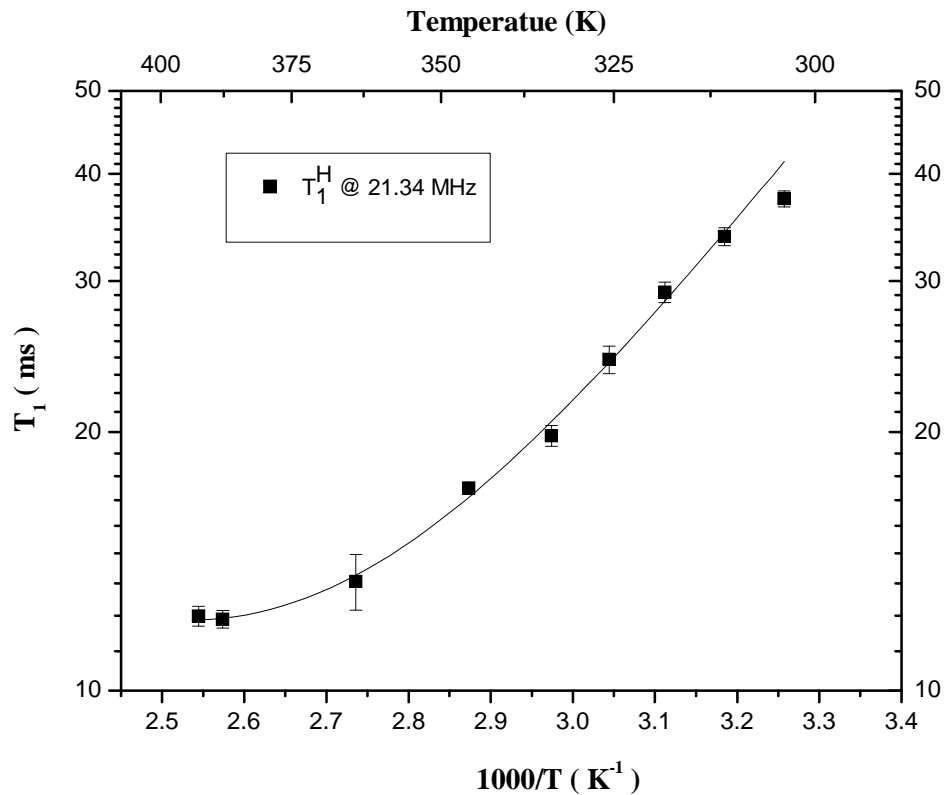


Figure 3.4 ¹H NMR T₁ data at 21.34 MHz for Ammonium zirconate in the high temperature region (> 300 K). Solid line shows the fit of T₁ data to Eqn. 3.1.

The spin lattice relaxation caused by translational diffusion using the random walk method by Torrey [51] has been described in Chapter 1. At high temperatures, when $\omega_0\tau \ll 1$, the relaxation rate due to translational diffusion is given by the Eqn. (1.65)

$$T_{1id}^{-1} = \left(\frac{8\pi N}{15a^3} \right) I(I+1)\gamma^4 \hbar^2 \left[\frac{\tau/2}{1 + (\omega\tau/2)^2} + \frac{\tau}{1 + \omega^2\tau^2} \right]. \quad (3.1)$$

The present high temperature T₁ data (> 300 K) is fit to the Eqn. (3.1) and is shown in the Fig. 3.4. The best fit parameters corresponding to the translational diffusion of the NH₄ ion are given in the Table 3.2. The activation energy E_a obtained for the translational diffusion is 23.2 (1) kJ/mol and the pre-exponential factor τ_{c0} is 8.8 (1) x 10⁻¹²s. These parameters compare with those reported for (NH₄) SnCl₃ [34].

Table 3.2 Motional Parameters for ammonium zirconate. The values given in parenthesis represent errors.

Mechanism	E _a (kJ/mol)	τ _{co} (s)
NH ₄ diffusion	23.2 (1)	8.8 (1) x 10 ⁻¹²
NH ₄ reorientation	13.6 (0.3)	19 (1) x 10 ⁻¹⁴

3.3.1.2 Intermediate temperature range (240 - 146 K)

Assuming that the NH₄ ion reorients in such a way that each proton spends the same amount of time at any of the hydrogen sites in the NH₄ tetrahedron, the proton relaxation time can be expressed using BPP approach as [1, 4, 52]

$$\left(T_1^{-1}\right)^H = \frac{27 \gamma^4 \hbar^2}{40 r^6} \left[\frac{\tau_H}{1 + \omega_H^2 \tau_H^2} + \frac{4 \tau_H}{1 + 4 \omega_H^2 \tau_H^2} \right], \quad (3.2)$$

where 'τ_H' represents the correlation time of the NH₄ motion and is assumed to obey the Arrhenius equation given by

$$\tau = \tau_0 \exp(E_a / RT) . \quad (3.3)$$

Here τ₀ and E_a are called pre-exponential factor and activation energy of the ammonium motion respectively. In Eqn. 3.2, γ = 2.675 x 10⁴ G⁻¹ s⁻¹ is the nuclear gyromagnetic ratio of proton and 'r' is the inter proton distance in the NH₄ tetrahedron.

The BPP model as given in Eqn. 3.2 fits well to the present experimental ¹H T₁ data in the temperature region 240 to 146 K as shown in the Fig. 3.5. The pre-exponential factor and activation energy found from the best fit are 19 (± 1) x 10⁻¹⁴ s and 13.6 (± 0.3) kJ/mol respectively. The ¹H second moment studies in the same compound [41] suggests that the activation energy corresponding the reorientation of the ammonium ion should be less than 17 kJ/mol. The activation energy obtained from the present investigation 13.6 kJ/mol and agrees with the reported prediction [41]. The observed motional parameters are in the same order of magnitude with other (NH₄)₂MCl₆ compounds [37, 53].

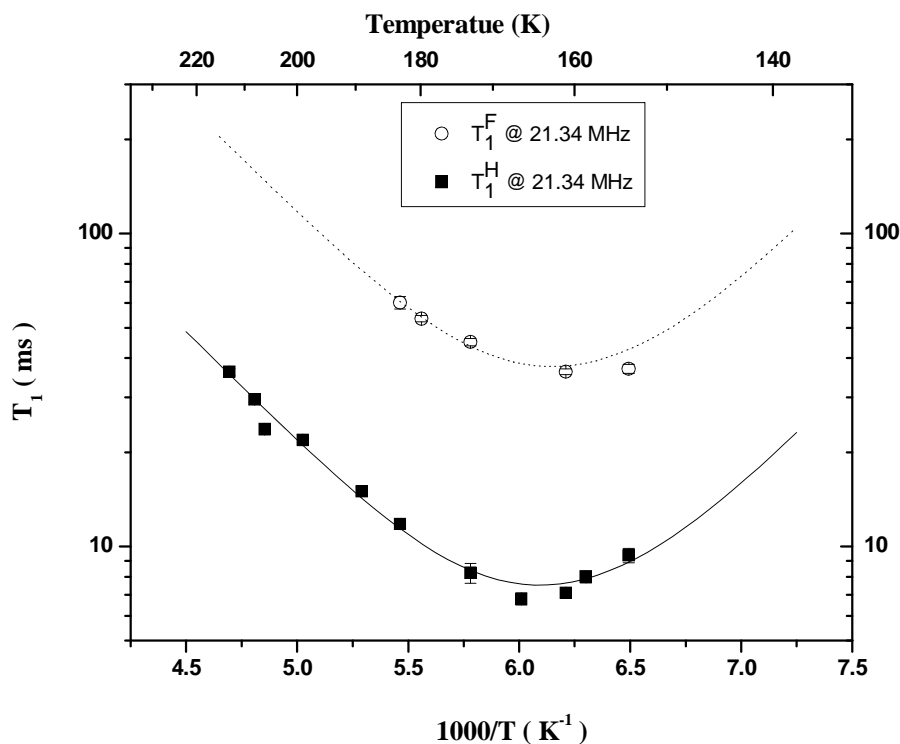


Figure 3.5 ^1H and ^{19}F T_1 data in the temperature range 220 – 146 K. Solid line represents the BPP fit to ^1H T_1 data and dotted line shows the simulated graph of BPP curve for ^{19}F T_1 data.

3.3.1.3 Low Temperature (LT) region (146 – 11 K)

The T_1 behaviour below 146 K, can be explained based on the quantum rotational tunneling of the ammonium ion. Lalowicz et al have also attributed the line shape of the proton NMR signal at 4.2 K to quantum rotational tunneling [28].

Theory

At lower temperatures, the rotational tunneling of the NH_4 ion becomes dominant. The observation of low activation energy for the reorientation of the NH_4 ion along with tunnelling at low temperatures has been reported by several authors [54 - 55]. The low hindering barrier in the case of NH_4 ion gives more freedom to the cation and at low

temperatures, it facilitates tunneling [56 - 57]. The Haupt's model [58] was modified by Koksai [54] to estimate the relaxation rate for the methyl group tunneling. Later Punkkinen [32] extended this model for ammonium ion. The four proton spins in an ammonium ion combine to form a five-fold degenerate A state ($I_{\text{tot}} = 2$), three sets of three – fold degenerate T states ($I_{\text{rot}} = 1$) and a doubly degenerate E state ($I_{\text{tot}} = 0$). The states are further split by the static magnetic field.

Assuming a very narrow tunnel-splitting distribution for ω_T and ω_E and that the torsional ground state is well separated from the first excited state, the relaxation rate can be given by [32],

$$\left(\frac{1}{T_1}\right)_{AT} = C_{AT} \left[\frac{\tau_T}{1 + \bar{\omega}_T^2 (\tau_T)^2} + \frac{\tau_T}{1 + (\bar{\omega}_T \pm \omega_o)^2 (\tau_T)^2} + \frac{\tau_T}{1 + (\bar{\omega}_T \pm 2\omega_o)^2 (\tau_T)^2} \right] \quad (3.4)$$

for the transitions between A and T states, where $\bar{\omega}_T$ is the average tunnel frequency for the A-T transitions. The three terms on the right-hand side correspond to the transitions $\Delta m = 0, \pm 1$ and ± 2 . Similarly, for the transitions between A and E states, the relaxation rate is given by

$$\left(\frac{1}{T_1}\right)_{AE} = C_{AE} \left[\frac{\tau_E}{1 + \bar{\omega}_E^2 (\tau_E)^2} + \frac{\tau_E}{1 + (\bar{\omega}_E \pm \omega_o)^2 (\tau_E)^2} + \frac{\tau_E}{1 + (\bar{\omega}_E \pm 2\omega_o)^2 (\tau_E)^2} \right] \quad (3.5)$$

the three terms in the relation corresponding to the transitions $\Delta m = 0, \pm 1$ and ± 2 . $\bar{\omega}_E$ is the average tunnel frequency for the A-E transitions.

The tunneling frequencies used in the Eqns. 3.4 and 3.5 can be approximately estimated from the value of observed $T_{1(\text{min})}$ (when $\omega_t \gg \omega_o$) using the relation [36]

$$\frac{T_{1(\text{min})}(\text{obs})}{T_{1(\text{min})}(\text{class})} \approx \frac{\bar{\omega}_T}{\omega_o} \quad (3.6)$$

This relation has been used in NH_4ClO_4 by Guttler and Von Schutz [29]. The relation (3.5) is reasonable if tunnel motion is considered to have a power spectrum centered around $\bar{\omega}_t$ instead of around $\omega = 0$ similar to the classical random motion.

In case of ammonium ion, an estimate of tunnel frequency can be made from the classical value of the $T_{1\text{min}}$ using the relation [32]

$$\bar{\omega}_t \approx 25.13 \times 10^9 T_{1(\min)} \text{ ,} \quad (3.7)$$

where $\bar{\omega}_t$ is in Hz when T_1 is in s. An empirical relation between the activation energy and the tunnel frequency can approximately given as [57]

$$\bar{\omega}_t \approx 26.5 \times 10^{12} \exp(-10.4\sqrt{E_a}) \text{ ,} \quad (3.8)$$

where $\bar{\omega}_t$ is in Hz when E_a is in kcal/mol.

Using the relations (3.6) or (3.7), an approximate estimate of tunnel frequency can be made and used in the equations (3.4) and (3.5) to give the best fit for the T_1 data at low temperatures and calculate the quantum parameters corresponding to the A-E or A-T transitions respectively.

When $\bar{\omega}_t \geq \omega_o$, the relations (3.5) and (3.6) can be modified as

$$\left(\frac{1}{T_1}\right)_{AT} = C_{AT} \left[\frac{\tau_T}{1 + \bar{\omega}_T^2 (\tau_T)^2} \right] \quad (3.9)$$

for A-T transition and

$$\left(\frac{1}{T_1}\right)_{AE} = C_{AE} \left[\frac{\tau_E}{1 + \bar{\omega}_E^2 (\tau_E)^2} \right] \quad (3.10)$$

for A-E transition. τ_T and τ_E follow the usual Arrhenius behaviour.

T_1 is found to be temperature independent, from 146 K down to 50 K, which suggests that only the ground tunnel state is occupied. Similar T_1 behaviour has been observed in many compounds at lower temperatures [34, 54, 59].

We have tried to fit the T_1 data below 28 K to the Eqn. of the form 3.10. and is shown in Figure 3.6. The tunnel frequency is estimated to be 405 MHz. The tunnel frequency measured in a few ammonium hexahalo metallates are found to vary over a wide range from 1.4 MHz to 600 MHz. [57]. The energy of the torsional splitting is estimated as 1.98 kJ/mol and the pre exponential factor is 8.38×10^{-15} s. On comparing the tunneling parameters with that of NH_4SnBr_3 , The observed tunnel frequency is higher than that of ‘A-T’ splitting and lower than that of ‘A-E’ tunnel splitting and activation torsional

splitting between the ground state and the first excited state which is 1.98 kJ/mol, fairly in agreement with that of ‘A-T’ tunneling.

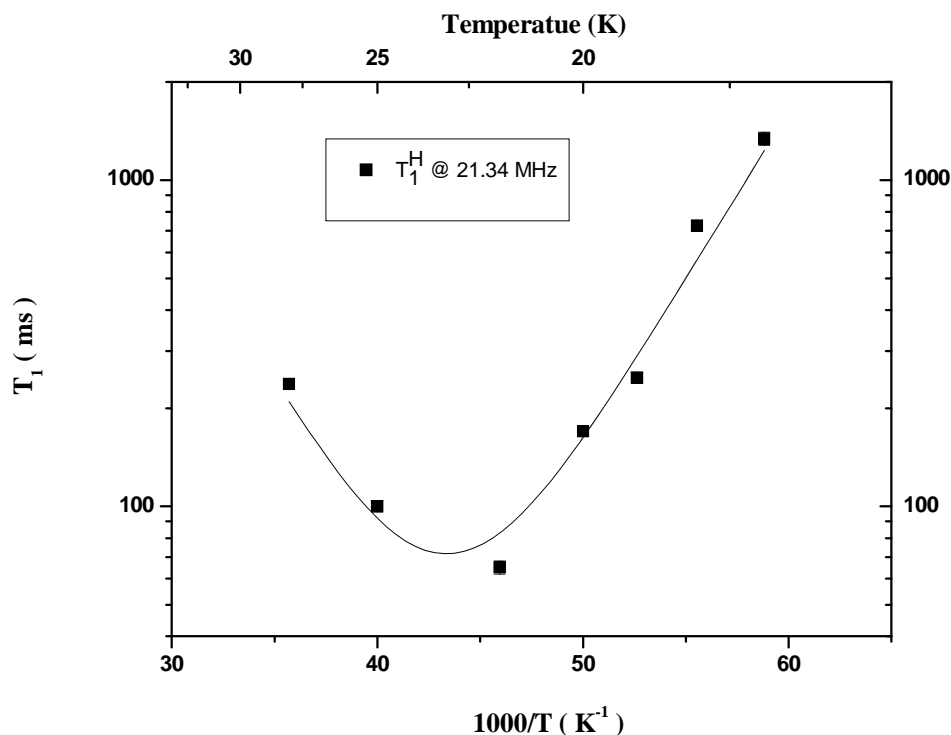


Figure 3.6 ^1H NMR T_1 data at 21.34 MHz for Ammonium zirconate in the temperature region (30 – 16 K). Solid line shows the fit of T_1 data to Eqn. 3.9.

3.3.2 Analysis of ^{19}F NMR T_1

^{19}F spin lattice relaxation time also shows similar behaviour as that of proton T_1 and is about 3 times more than that of proton. At room temperature T_1 value is about 48 ms and on increasing the temperature, it starts decreasing up to 395 K, above which it reduces sharply to less than a millisecond similar to proton T_1 . In the same temperature region, FID duration also increases a few times as the temperature is increased from 388 K to 410 K. On decreasing the temperature from room temperature, initially T_1 increases and shows a relatively broad maximum (as compared to that of proton) of about 60 ms around 220 K. Below 200 K, T_1 decreases and follows through a shallow minimum of about 35

ms around 160 K (at which proton minimum is also observed). Below 160 K, Fluorine T_1 again goes through another minimum of 19.7 ms and then increases to about 31 ms at 106 K. Below this temperature, T_1 remains constant (within experimental error) till about 50 K and on further reducing temperature T_1 again increases monotonically to about 500 ms at 20 K. Below 20 K signal could not be measured due to poor signal to noise ratio till the lowest temperature of measurement (11 K).

3.3.2.1 High Temperature (HT) region (410 - 240 K)

In the temperature range 120-200 K, the ^{19}F wide-line NMR signal [41] has shown a single asymmetric line and in the range 210 - 275 K the spectrum has shown a number of components with different widths and above 275 K the additional peaks have disappeared. The complexity of the ^{19}F NMR spectrum are due to polymeric nature of $(\text{NH}_4)_2\text{ZrF}_6$ makes it difficult to understand the NMR data. With further increase in temperature, the width of the line has decreased and around 340 K a new transformation of the signal starts and completes above 400 K by the formation of an asymmetric narrow line with fine structure. The phase transformation of Ammonium zirconate in the temperature range 410 - 415 K has not changed the line shape. Hence, the analysis of the ^{19}F T_1 is similar to that of proton. Both decrease in T_1 and narrowing of the NMR signal may be attributed to diffusion of both F ions through the lattice. High ionic conductivity above 400 K observed by Kavun et al [47] supports this. Sub lattice movement of F ions is also observed above 400 K [47]. The observed maximum in fluorine T_1 in the present study around room temperature may be attributed to the competition between diffusion and reorientational motion.

3.3.2.2 Intermediate temperature range (200- 106 K)

^{19}F T_1 data in this temperature region also appears to follow the BPP model and fit of the linear portion of the ^{19}F T_1 data in this region gives the activation energy of 13 (± 1) kJ/mol and is attributed to reorientation of the ammonium group. Hence it is concluded that, the ammonium ion reorientations are rate determining and the fluorines relax to the lattice mainly by the random modulations of the H - F dipole-dipole interactions due to NH_4 motion. Several authors have observed similar behaviour in a

number of compounds, for example, Watton et al [53] in $(\text{NH}_4)_2\text{TiF}_6$, McDowell et al [60] in $(\text{CH}_3)_3\text{NPF}_5$ and explained their results in the similar manner. Indeed, Kavun et al have also observed that in the present compound, ^{19}F second moment reaches the rigid lattice limit at much higher temperature of about 250 K. Fig 3.4 shows the BPP fit to ^1H T_1 data and simulated graph of BPP curve for ^{19}F T_1 is also shown.

3.3.2.3 Low temperature range (106 - 20 K)

Fluorine T_1 data in this temperature range is also attributed to the onset of ammonium ion motion as second moment studies in the same compound have shown that the fluorine motions freeze at much higher temperatures at least in the NMR time scale.

3.3 Conclusion

The present investigation reveals that in Ammonium zirconate, ammonium ion plays a major role in relaxation mechanism in the present temperature range of study. At higher temperature, the compound shows diffusion of both ammonium and fluorine sub lattice. Sharp increase of FID duration and sudden increase of relaxation rate around 395 K, is supported by other techniques such as wide-line NMR line shape, second moment as well as the conductivity studies. Further, this investigation reveals the reorientational motion of the ammonium ion is responsible for fluorine relaxation also. Another important observation is that even at low temperatures the fluorine nuclei are being relaxed due to quantum rotational tunneling of the ammonium ion. Superionic conductivity in the sample is interpreted as due to the NH_4 ion and fluorine sublattice motion.

References

1. Bloembergen N, Purcell EM, Pound RV. *Phys. Rev.*, **73 (7)**, 679 (1948).
2. Hubbard PS. *Phys. Rev.*, **131**, 1155 (1963).
3. Torrey HC. *Phys. Rev.*, **76**, 1059 (1949).
4. Abragam A, *The Principles of Nuclear Magnetism*. Oxford University Press; New York, **1961**.
5. Ikeda I and McDowell. *Mol. Phys.*, **25**, 1217 (1973).
6. Punkkinen M, Tuohi JE and Ylinen EE. *J. Magn. Reson.*, **22**, 527 (1976).
7. Svare I. *J. Phys. C: Solid State Phys.*, **12**, 3907 (1979).
8. Prager M, Raaen AM and Svare I. *J. Phys. C: Solid State Phys.*, **16**, L181 (1983).
9. Pelzl J and Dimitropoulos C. *Z. Naturforsch.*, **49a**, 232 (1994).
10. Armstrong RL, Van Driale HM and Sharp AR. *Can. J. Phys.*, **52**, 369 (1974).
11. Tegenfeldt J and Odberg L. *J. Phys. Chem. Solids*, **33**, 215 (1972).
12. Watton A, Sharp AR, Petch HE and Pintar MM. *Phys Rev.*, **5B**, 4281 (1979).
13. Kodama T. *J Magn. Reson.*, **7**, 137 (1972).
14. Ylinen EE, Tuohi JE and Niemela LKE. *Chem. Phys. Lett.*, **24**, 447 (1974).
15. Ingman LP, Koivula, Lalowicz ZT, Punkkinen M and Ylinen EE. *Z. Phys. B Cond. Matt*, **81**, 175 (1990).
16. De Wit GA and Bloom M. *Can. J. Phys.*, **47**, 1195 (1969).
17. Murthy BVS. *Ph.D. thesis*, Department of Physics, Indian Institute of Science, Bangalore, India, **1993**.
18. Bonori M and Terenzi M. *Chem. Phys. Lett.*, **27**, 281 (1974).
19. Watton A. *J. Chem. Phys.*, **65**, 3653 (1976).
20. Prager M and Heidemann A. *ILL Report*, **87PR15T**, Table 13 (1987).
21. Srinivasan R. *MTP International Review of Science*, Physical Chemistry, Series 2, Butterworths, London, **4**, 209 (1975).
22. Clough S. *Physica*, **136B**, 145 (1986).
23. Clough S, Horsewill AJ, Johnson MR, Mohammed MA and Newton T. *Chem. Phys.*, **152**, 343 (1991).
24. Clough S. *Encyclopedia of NMR*, Eds. Grant DM and Harris RK, **6**, 3933 (1996).
25. Horsewill AJ. *Spectrochim. Acta*, **48A**, 379 (1992).

26. Horsewill AJ, *Prog. Nucl. Magn. Reson. Spectr.* **35**, 359 (1999).
27. Watton A and Petch EA. *Phys. Rev.*, **B7**, 6 (1973).
28. Lalowicz ZT, McDowell CA and Raghunathan P. *J. Chem. Phys.*, **70**, 4819 (1979).
29. Guttler W and Von Schutz JU. *Chem. Phys. Lett.*, **20**, 133 (1973).
30. Riehl JW, Wang R and Bernad HW. *J. Chem. Phys.*, **58**, 509 (1973).
31. Nijman AJ, Sprik M and Trappeniers NJ. *Physica*, **98B**, 247 (1980).
32. Punkkinen M. *J. Magn. Reson.*, **19**, 222 (1975).
33. Tuohi JE, Ylinen EII and Niemela LKE. *Magn. Reson. And Rel. Phenomena*, **2**, Proc. 18th Ampere congress, Nottingham, 1974, eds Allen PS, Andrew ER and bates CA. North- Holland Publ.Co., Amsterdam, 399 (1975).
34. Senthil Kumaran S. *Ph.D. thesis*, Department of Physics, Indian Institute of Science, Bangalore, India, **1997**.
35. Punkkinen Ma and Clough S. *J. Phys. C: Solid State Phys.*, **8**, 2159 (1975).
36. Svare I and Tunstall DP. *J. Phys. C: Solid State Phys.*, **8**, L559 (1975).
37. Svare I, Raaen AM and Thorkildsen G. *J. Phys. C: Solid State Phys.*, **11**, 4059 (1978).
38. United States Patents: 20030171524, 6730746, 3130188, 5932512, 6838533, 6716569 and 4,391,652.
39. Allan Zalkin, David Eimerl and Velsko SP. *Acta Cryst.*, **C44**, 2050 (1988).
40. Annalize Kruger and Heyns AM.: *Vibra. Spectro.*, **14**, 171 (1997).
41. Kavun VYa, Sergienko VI, Chernyshov BN, Bukvetskii BV, Dedenko NA, Bakeeva NG and Ignat'eva LN. *Russ. J. Inorg. Chem.* **36 (4)**, 570 (1991).
42. Lane AP and Sharp DWA. *J. Chem. SOC. (A)*, **2942** (1969)
43. Kavun VYa, Didenko NA, Slobodyuk AB Tkachenko IA, Gerasimenko AV, Uvarov NF and Sergienko VI. *J. Struct. Chem.* **46 (5)**, 839 (2005).
44. Voit EI, Voit AV, Kavun Vya and Sergienko VI. *J. Struct. Chem.*, **45(4)**, 610 (2004).
45. Gordienko PS, Vasil'ev AM and Epov DG. *Russ. J. Physical Chem.*, **56**, 542 (1982).
46. Epov DG and Mikhailov MA. *Russ. J. Inorg. Chem.* **22(4)**, 534 (1977).

47. Kavun VYa, Uvarov NF, Slobodyuk AB, Goncharuk VK, Kotenkov AYu, Tkachenko IA, Gerasimenko AV and Sergienko VI. *Russ. J. Electrochem.*, **41 (5)**, 501 (2005).
48. Rodriguez AM, Martinez JA, Caracoche MC, Rivas PC and Lopez Garcia AR. *Hyperfine Interactions*, **14**, 227 (1983).
49. Rodriguez AM, Martinez JA, Caracoche MC, Rivas PC, Lopez Garcia AR and Spinelli S. *J. Chem. Phys.*, **82 (3)**, 1271 (1985).
50. A. M. Heyns, K. R. Hirsch, and W. B. Holzapfel. *J. Chem. Phys.*, **73 (1)**, 105 (1980).
51. Torrey HC. *Phys. Rev.*, **92(4)**, 962 (1953).
52. Blinc R and Lahajnar G. *J. Chem. Phys.* **47 (10)**, 4146 (1967).
53. Wattton A, Koster E, Sandu HS and Petch HE. *J. Chem. Phys.* **70 (11)**, 5197 (1979).
54. Köksal F, Rössler E and Sillescu H. *J. Phys. C: Solid State Phys.*, **15**, 5821 (1982).
55. Allen PS and Snell AJ. *J. Phys. C: Solid State Phys.*, **6**, 3478 (1973).
56. Tuohi JE, Ylinen EII. *Phys. Scr.*, **13**, 253 (1976).
57. Svare I. *J. Phys. C: Solid State Phys.*, **10**, 2679 (1977).
58. Haupt J. *Z. Naturforsch.*, **26a**, 1578 (1971).
59. Senthil Kumaran S, Ramesh KP and Ramakrishna J. *Mol. Phy.*, **99(16)**, 1373 (2001).
60. McDowell CA, Raghunathan P and Williams DS. *J. Magn. Reson.*, **32**, 57 (1978).